The following publication X. Luo, S. Niu and W. N. Fu, "Design and Sensorless Control of a Novel Axial-Flux Permanent Magnet Machine for In-Wheel Applications," in IEEE Transactions on Applied Superconductivity, vol. 26, no. 7, pp. 1-5, Oct. 2016 is available at https://doi.org/10.1109/TASC.2016.2594862

Design and Sensorless Control of a Novel Axial-Flux Permanent Magnet Machine for In-Wheel Applications

Xiang Luo, Shuangxia Niu, and W. N. Fu

***Abstract*—This paper proposes an axial-flux-modulation permanent magnet (PM) machine and its sensorless control strategy for in-wheel application in electrical vehicles. A Vernier structure is integrated with the axial-flux PM machine to include the magnetic gear effect and improve output torque. The sensorless control strategy of the proposed machine, including initial rotor position estimation and rotating position estimation, is proposed for flux-modulation motors in this paper. The initial rotor position estimation is based on the technique of rectangular pulse voltage injection and the rotating rotor position estimation is based on the sliding mode observer (SMO). The saturation effect on inductances, which is the theoretical basis of the rectangular pulse voltage injection, makes the stator parameter variation in different loads and affects the SMO estimation. To overcome this problem, a novel online parameter self-adjustment procedure for the SMO is introduced. The machine design and its sensorless control performance are verified by simulation and prototype experiments.**

***Index Terms*—Axial flux permanent magnet (PM) machine, inductance saturation effect, initial rotor position, parameter self-adjustment, sliding mode observer (SMO), Vernier structure.**

I. Introduction

AXIAL-FLUX permanent magnet (PM) machines are widely used in electrical vehicles as their high power density and high efficiency [1], [2]. They are very suitable to be mounted in wheels of electric vehicles or hybrid electric vehicles for direct drives due to their compact structure and short axial length. In this paper, a Vernier structure is integrated with the axial-flux PM machine to include the flux-modulation effect, which contributes to improve output torque for the in-wheel drives [3]. The proposed axial-flux Vernier PM direct-drive machine (AFVPMM) is especially suitable for in-wheel applications because its stator windings have a fractional slot concentrated distribution and phase inductance is increased accordingly. The bigger inductance is relatively easy to be calculated and helps to improve the flux weakening capability of machine [4].

This work was supported by the Research Grant Council of the Hong Kong Government under Project PolyU 152130/14E.

X. Luo is with Hong Kong Polytechnic University, Hung Hom, Hong Kong, and also with Shanghai Jiaotong University, Shanghai 200240, China (e-mail: maskluo@sjtu.edu.cn).

S. Niu and W. N. Fu are with Hong Kong Polytechnic University, Hung Hom, Hong Kong (e-mail: eesxniu@polyu.edu.hk; eewnfu@polyu.edu.hk).

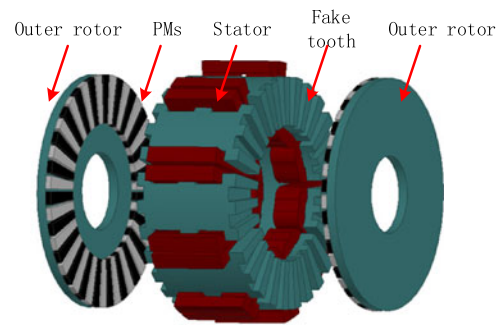

Fig. 1. Structure of the proposed machine.

For in-wheel applications, motors always suffer from the poor operating environments and the limitation of installation space, which cause the position sensors such as optical encoders or resolvers not suitable to be installed in limited space. In this paper, the sensorless control strategy of the proposed machine is presented. In order to accurately estimate the initial rotor position of the proposed AFVPMM, an improved pulse voltage vector injection strategy is proposed. The response currents of the injected pulse voltage are different from each other due to the difference of the magnetic saturation caused by the magnetic saliency [5]. The voltage vector angle is required to be divided continuously for high-precision so that larger angle errors can be reduced to a certain value. The rotating position estimation is based on the sliding mode observer (SMO), which has been proved as one of the most effective estimation method for traditional PM synchronous machines [6]–[11]. The magnetic saturation effect helps to evaluate the initial rotor position, but affects the SMO estimation due to the variation of the stator parameters in different loads. In this paper, an iterative stator self-adjustment procedure is introduced to solve the parameter change problem. The proposed motor design and its sensorless control strategy are verified by the simulation and experimental results.

II. Proposed Machine and Analysis

A. Proposed Machine

As shown in Fig. 1, in order to improve the torque density, dual-rotor structure is used in the proposed AFVPMM. The machine has two air gaps, 23 pole pairs of surface mounted PMs on the two sides of the rotor, 4 pole-pair, 9 slot winding armatures with 27 stator teeth in the stator. The rated speed of the machine

TABLE I
SPECIFICATIONS OF THE PROPOSED AFVPMM

Parameter	Value
Input voltage (V)	155
Rated torque (Nm)	8
Rated speed (rpm)	400
Outer diameter of stator and rotor (mm)	60
Inner diameter of rotor (mm)	20
Inner diameter of stator (mm)	35
Stator thickness (mm)	50
Axial length of rotor PMs (mm)	25
PM thickness (mm)Air-gap length (mm)	31
Turn number per phase	45
Rotor pole-pair number	23
Stator pole-pair number	4
Stator fake tooth number	27

is 400 rpm and rated torque is 8 Nm. A significant improvement in the flux weakening capability can be achieved by employing fractional slot concentrated windings [4]. So the combination of 8 poles / 9 slots fractional slot concentrated winding is used in the proposed machine. Table I lists the specifications of the proposed AFVPMM. Compared with conventional radial flux machines, although the manufacturing and the material cost is relatively high, the torque density can be improved.

The modulation effect is integrated to the machine with the fake teeth on both sides of the stator. The flux made by the stator armature winding whose pole-pair number is 4 is modulated by the 27 stator fake teeth, the 23 pole-pair harmonic becomes the main flux component, which equals to the rotor pole-pair number. The modulated stator flux and the PM flux interacts in the airgap so that the proposed machine works. This working principle is as the same as the magnetic gears [12], and the ratio G_r for speed and torque is given by

$$G_r = \frac{|p_s - N_s|}{p_s} \tag{1}$$

where N_s is the number of flux-modulation fake tooth poles and p_s is the number of armature winding pole-pairs. In this paper, $N_s = 27$ and $p_s = 4$. The stator flux rotating speed ω_s, rotor speed ω_r have the relationship as

$$G_r = -\omega_s/\omega_r = -23/4. \tag{2}$$

This means that the rotor speed is only 4/23 of that in the conventional machine with the same number of armature winding poles, but the rotor rotates in an opposite direction.

B. Finite Element Model (FEM) Analysis

The 3-D FEM is used to analyze the proposed AFVPMM. Fig. 2(a) shows the FFT analysis results of the magnetic flux density in the airgap. It can be seen that the 23 pole-pair number component is the main one and significantly higher than the other flux density components. Fig. 2(b) shows the no-load back EMF at rated speed which is used to verify the machine design. Fig. 2(c) shows the electromagnetic torque versus angle characteristics of the proposed machine. The result shows a fine sinusoidal output and small harmonic contents. Fig. 2(d) shows

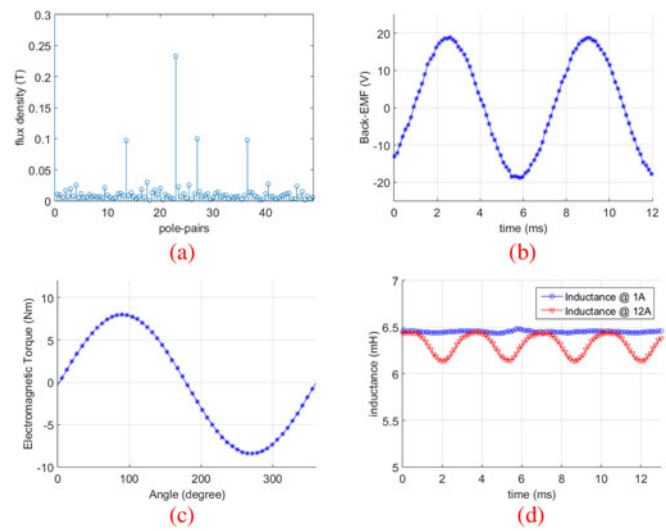

Fig. 2. FEM analysis results. (a) FFT result of the flux density in the air gap. (b) No-load back EMF at 400 rpm. (c) Electromagnetic torque versus angle characteristic. (d) Phase-A self-inductance.

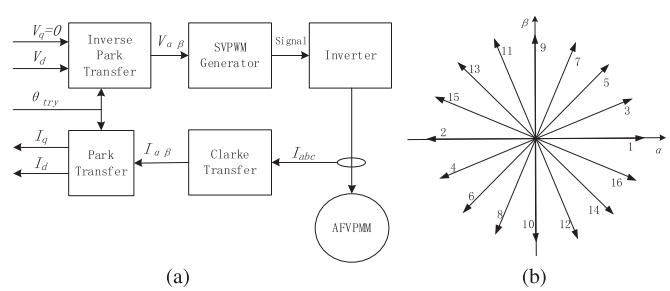

Fig. 3. Initial position estimation for the proposed machine. (a) Estimation diagram. (b) Voltage vectors.

the inductance value of phase A under different loads. The result shows significant variation of the inductance value. When current increases, the inductance of phase A tends to be saturated, which causes the variation of inductance, which indicates the necessity to find improved sensorless control strategy for the proposed machine.

III. SENSORLESS CONTROL STRATEGY

A. Initial Position Estimation

As shown in Fig. 2(d), the inductance changes when the stator current changes, which proves the magnetic saturation effect on the proposed machine. When the rotor holds still, the d-axis inductance will smaller than the q-axis inductance when the current is large. If rectangular pulse voltage injected into the machine with different vector direction, different feedback currents are received. Fig. 3(a) shows the initial rotor position estimation diagram.

Fig. 3(b) shows the sketch map of the directions of the pulse voltage vectors. In the sketch map, 16 distinct voltage vectors are injected into the motor in numerical order. In this paper, 64 distinct vectors are selected in the same way for accuracy.

Each voltage vector has the interval of 5.625° electrical degrees and retains the same action time. The current response of each voltage vector is calculated and the subtraction result of the opposite vector is recorded. The maximum subtraction result represents the pair of the vectors are on the d-axis and the minimum result represents the q-axis.

B. Rotating Position Estimation

The $\alpha-\beta$ axis voltage equations of the stator can be described by the following equations:

$$\begin{bmatrix} \frac{di_\alpha}{dt} \\ \frac{di_\beta}{dt} \end{bmatrix} = \begin{bmatrix} \frac{-R}{L} & 0 \\ 0 & \frac{-R}{L} \end{bmatrix} \begin{bmatrix} i_\alpha \\ i_\beta \end{bmatrix} + \begin{bmatrix} \frac{1}{L} & 0 \\ 0 & \frac{1}{L} \end{bmatrix} \begin{bmatrix} v_\alpha \\ v_\beta \end{bmatrix} + \begin{bmatrix} -\frac{1}{L} & 0 \\ 0 & -\frac{1}{L} \end{bmatrix} \begin{bmatrix} e_{\alpha 1}+e_{\alpha 2} \\ e_{\beta 1}+e_{\beta 2} \end{bmatrix} \tag{3}$$

where $i_{\alpha,\beta}$ and $v_{\alpha,\beta}$ represent the current and voltage for each axis, $e_{\alpha 1,\beta 1}$ and $e_{\alpha 2,\beta 2}$ represent the back electromotive force related by the two rotors, and *R* and *L* represent the stator resistance and inductance. The electromotive force for each side can be represented in the stationary frame as

$$\begin{bmatrix} e_{\alpha x} \\ e_{\beta x} \end{bmatrix} = \begin{bmatrix} \lambda_{sx} G_r \omega_r & 0 \\ 0 & -\lambda_{sx} G_r \omega_r \end{bmatrix} \begin{bmatrix} \sin\theta \\ \cos\theta \end{bmatrix} \tag{4}$$

where $x = 1, 2$ represent the two rotors, λ_{sx} is the magnetic flux created by the PMs in the rotor modulated by the stator tooth; and θ is the stator rotating flux position. As the back EMFs contain the position information, a SMO is used to estimate the rotating flux position. According to the voltage balance equation, the SMO based estimation equation is

$$\begin{bmatrix} \frac{d\hat{i}_\alpha}{dt} \\ \frac{d\hat{i}_\beta}{dt} \end{bmatrix} = \begin{bmatrix} \frac{-R}{L} & 0 \\ 0 & \frac{-R}{L} \end{bmatrix} \begin{bmatrix} \hat{i}_\alpha \\ \hat{i}_\beta \end{bmatrix} + \begin{bmatrix} \frac{1}{L} & 0 \\ 0 & \frac{1}{L} \end{bmatrix} \begin{bmatrix} v_\alpha \\ v_\beta \end{bmatrix} + \begin{bmatrix} -\frac{1}{L} & 0 \\ 0 & -\frac{1}{L} \end{bmatrix} \begin{bmatrix} kZ\left(\tilde{i}_\alpha\right) \\ kZ\left(\tilde{i}_\beta\right) \end{bmatrix} \tag{5}$$

where the symbol "^" represents the estimated value, $\tilde{i}_s = \hat{i}_s - i_s$, in which subscript s represents α and β and *k* is the sliding mode gain value. The switching function $Z(\tilde{i}_s)$ is used to change the estimation system states to ensure that the estimation process is on the sliding surface, which is represented as

$$Z\left(\tilde{i}_s\right) = 2/(1+e^{-\tilde{i}_s}) - 1. \tag{6}$$

Considering the stator parameter change, the *R* and *L* can be changed to $\hat{R}$ and $\hat{L}$ in Eq. (5), which represents the estimated value of real changed stator resistance and inductance. The iterative parameter self-adjustment procedure of the SMO can be derived during the stability analysis. The stability of the proposed SMO can be proved by the Lyapunov function analysis. Define $S_n = [\,S_\alpha\ S_\beta\,]^T$, in which $S_\alpha = \tilde{i}_\alpha = \hat{i}_\alpha - i_\alpha$, $S_\beta = \tilde{i}_\beta = \hat{i}_\beta - i_\beta$. Defining $A = 1/L$ for simplification, the extended Lyapunov function used to find the sliding condition and parameter self-adjustment can be expressed as

$$V = \frac{1}{2} S_n^T S_n + \frac{1}{2}\left(\hat{A} - A\right)^2 + \frac{1}{2}\left(\hat{R} - R\right)^2. \tag{7}$$

From the Lyapunov stability theorem, the sliding mode condition can be derived to satisfy the condition that $dV/dt < 0$ for $V > 0$. The derivative of *V* is

$$\frac{dV}{dt} = [\,S_\alpha\ S_\beta\,]\,\frac{dS}{dt} + \left(\hat{A} - A\right)\frac{d\hat{A}}{dt} + \left(\hat{R} - R\right)\frac{d\hat{R}}{dt}. \tag{8}$$

The derivatives of the estimated phase current is

$$\begin{aligned} \frac{dS_s}{dt} &= \frac{d\tilde{i}_s}{dt} = \frac{d\hat{i}_s}{dt} - \frac{di_s}{dt} \\ &= -\left(\hat{R} - R\right)\hat{A}\hat{i}_s + \left(\hat{A} - A\right)\left(v_s - R\hat{i}_s\right) \\ &\quad - AR\tilde{i}_s + Ae_s - \hat{A}kZ\left(\tilde{i}_s\right) \end{aligned} \tag{9}$$

where s represents α and β. By substituting (9) to (8), the sliding condition can be represented as

$$\begin{aligned} \frac{dV}{dt} &= [\,\tilde{i}_\alpha\ \tilde{i}_\beta\,] \\ &\quad \times \begin{bmatrix} \begin{pmatrix} -\left(\hat{R} - R\right)\hat{A}\hat{i}_\alpha + \left(\hat{A} - A\right)\left(v_\alpha - R\hat{i}_\alpha\right) \\ -AR\tilde{i}_\alpha + Ae_\alpha - \hat{A}kZ\left(\tilde{i}_\alpha\right) \end{pmatrix} \\ \begin{pmatrix} -\left(\hat{R} - R\right)\hat{A}\hat{i}_\beta + \left(\hat{A} - A\right)\left(v_\beta - R\hat{i}_\beta\right) \\ -AR\tilde{i}_\beta + Ae_\beta - \hat{A}kZ\left(\tilde{i}_\beta\right) \end{pmatrix} \end{bmatrix} \\ &\quad + \left(\hat{A} - A\right)\frac{d\hat{A}}{dt} + \left(\hat{R} - R\right)\frac{d\hat{R}}{dt} < 0. \end{aligned} \tag{10}$$

To satisfy the condition of (10), it can be decomposed into three parts as follows:

$$[\,\tilde{i}_\alpha\ \tilde{i}_\beta\,] \begin{bmatrix} \left(\hat{A} - A\right)\left(v_\alpha - R\hat{i}_\alpha\right) \\ \left(\hat{A} - A\right)\left(v_\beta - R\hat{i}_\beta\right) \end{bmatrix} + \left(\hat{A} - A\right)\frac{d\hat{A}}{dt} = 0 \tag{11}$$

$$[\,\tilde{i}_\alpha\ \tilde{i}_\beta\,] \begin{bmatrix} -\left(\hat{R} - R\right)\hat{A}\hat{i} \\ -\left(\hat{R} - R\right)\hat{A}\hat{i}_\beta \end{bmatrix} + \left(\hat{R} - R\right)\frac{d\hat{R}}{dt} = 0 \tag{12}$$

$$[\,\tilde{i}_\alpha\ \tilde{i}_\beta\,] \begin{bmatrix} -AR\left(\hat{i}_\alpha - i_\alpha\right) + Ae_\alpha - \hat{A}kZ\left(\hat{i}_\alpha - i_\alpha\right) \\ -AR\left(\hat{i}_\beta - i_\beta\right) + Ae_\beta - \hat{A}kZ\left(\hat{i}_\beta - i_\beta\right) \end{bmatrix} < 0. \tag{13}$$

From the condition used to satisfy (11) and (12), the estimations of the stator inductance and resistance are obtained as

$$\frac{d\hat{A}}{dt} = R\left(\tilde{i}_\alpha \cdot \hat{i}_\alpha + \tilde{i}_\beta \cdot \hat{i}_\beta\right) - v_\alpha \cdot \tilde{i}_\alpha - v_\beta \cdot \tilde{i}_\beta \tag{14}$$

$$\frac{d\hat{R}}{dt} = \hat{A}\left(\tilde{i}_\alpha \cdot \hat{i}_\alpha + \tilde{i}_\beta \cdot \hat{i}_\beta\right). \tag{15}$$

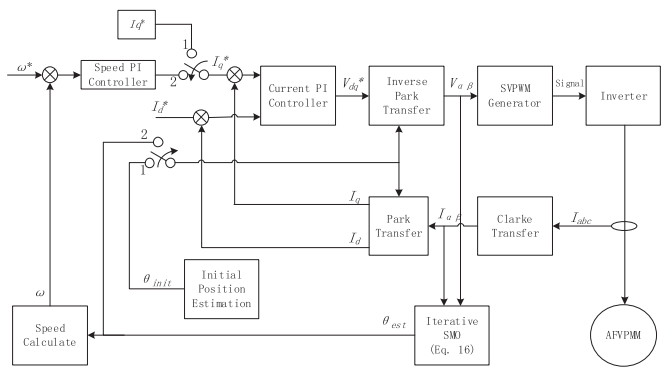

Fig. 4. Sensorless control strategy block diagram of the AFVPMM.

According to (14), $\hat{A}$ can be derived by an initial value of R. After $\hat{A}$ finishes its estimation, $\hat{R}$ can be derived by $\hat{A}$ according to (15).

To satisfy the inequation (13), the value of the SMO gain k should satisfy $k > \mathrm{MAX}(\frac{\hat{L}}{L}|e_\alpha|, \frac{\hat{L}}{L}|e_\beta|)$. When estimated inductance $\hat{L}$ is close to the real value L, the equation can be simplified as $k > \mathrm{MAX}(|e_\alpha|, |e_\beta|)$.

The rotating position estimation is concluded as follows:

$$\begin{cases} \dot{\hat{i}}_\alpha = -\hat{R}\hat{A}\hat{i}_\alpha + \hat{A}V_\alpha - k\hat{A}Z(\tilde{i}_\alpha) \\ \dot{\hat{i}}_\beta = -\hat{R}\hat{A}\hat{i}_\beta + \hat{A}V_\beta - k\hat{A}Z(\tilde{i}_\beta) \\ \dot{\hat{e}}_\alpha = kZ(\tilde{i}_\alpha) \\ \dot{\hat{e}}_\beta = kZ(\tilde{i}_\beta) \end{cases}$$

$$\begin{cases} \dfrac{d\hat{A}}{dt} = R\left(\tilde{i}_\alpha \cdot \hat{i}_\alpha + \tilde{i}_\beta \cdot \hat{i}_\beta\right) \\ \qquad\qquad - v_\alpha \cdot \tilde{i}_\alpha - v_\beta \cdot \tilde{i}_\beta \\ \dfrac{d\hat{R}}{dt} = \hat{A}\left(\tilde{i}_\alpha \cdot \hat{i}_\alpha + \tilde{i}_\beta \cdot \hat{i}_\beta\right). \end{cases} \tag{16}$$

C. Sensorless Control Strategy

The whole sensorless control strategy is proposed as shown in Fig. 4. After the estimation of the initial rotor position, the I/F control scheme is used for starting and low speed operation of AFVPMM. When the speed of the motor reaches a certain frequency, the SMO are integrated and used as the position feedback of the machine.

IV. Experimental Results

The proposed machine and the experimental setup are shown in Fig. 5. The machine is connected with a 1.5 kW separately excited DC motor which is used as prime movers in back-EMF measurement and as load in the control experiments.

The measured back-EMF at the rated speed is shown in Fig. 6, the line back-EMF peak-peak voltage is 62V, which agrees with the simulation result shown in Fig. 2(b). The sensorless control experiment results are shown in Fig. 7. The initial rotor position procedure is shown in Fig. 7(a) and (b). In Fig. 7(a), the current feedback of phase A is recorded, and the calculation result of the I_d subtraction is shown in Fig. 7(b). The voltage injection order is discussed in Section III, Part A. It can be seen from the picture that the 32 subtraction results are essentially sinusoidal, the minimum result is close to zero which indicates the q-axis direction and the maximum result indicates the d-axis.

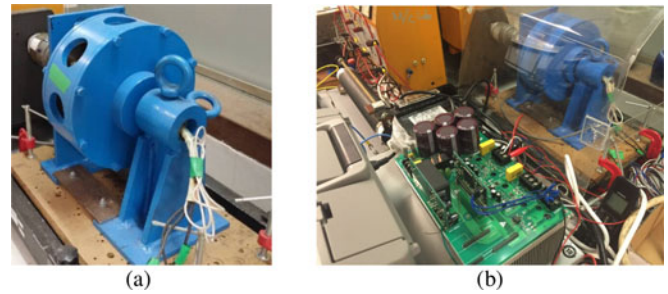

Fig. 5. Experimental system. (a) Proposed machine. (b) Controller.

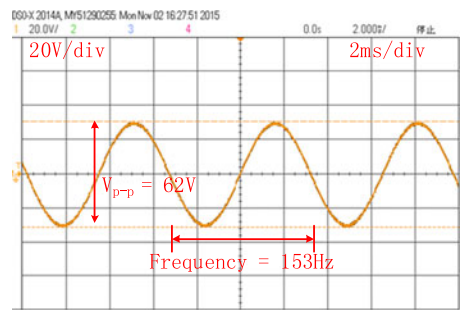

Fig. 6. Measured no-load back-EMF at the rated speed.

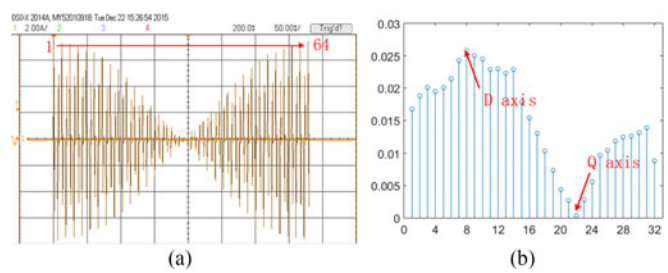

Fig. 7. Measured sensorless control results. (a) Phase-A current response at initial rotor position estimation. (b) Calculated I_d subtraction result at initial rotor position estimation.

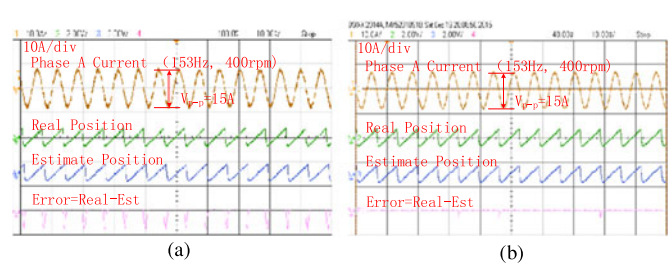

Fig. 8. Heavy load SMO based sensorless control at rated speed. (a) Without parameter self-adjustment. (b) With parameter self-adjustment.

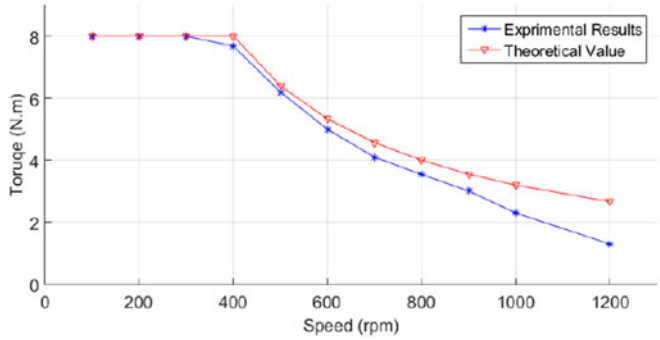

Fig. 9. Flux weakening results.

The SMO based rotating estimate results at the rated speed are shown in Fig. 8(a) and (b). Fig. 8(a) and (b) shows the results without/with parameter estimation, separately. It can be seen in Fig. 8(a), the estimation error is significant. With the iterative parameter self-adjustment procedure, the error of the estimation in Fig. 8(b), is very small. Fig. 9 shows the flux weakening results of the proposed machine. Thanks to the fractional slot concentrated winding connection, the machine can get 3 times of the rated speed.

V. Conclusion

The proposed novel AFVPMM shows its good flux weakening performance and high torque density which are verified by the simulation results and experimental results. The sensorless control strategy including standstill initial positon estimation and SMO based parameter self-adjustment rotating position estimation is also proposed in the paper. The control strategy of the machine is verified by the experiments.

References

[1] C. Liu, J. Zhong, and K. T. Chau, "A novel flux-controllable Vernier permanent-magnet machine," *IEEE Trans. Magn.*, vol. 47, no. 10, pp. 4238–4241, Oct. 2011.

[2] C. Liu, K. T. Chau, J. Z. Jiang, and L. Jian, "Design of a new outer-rotor permanent magnet hybrid machine for wind power generation," *IEEE Trans. Magn.*, vol. 44, no. 6, pp. 1494–1497, Jun. 2008.

[3] S. L. Ho, S. Niu, and W. N. Fu, "Design and comparison of Vernier permanent magnet machines," *IEEE Trans. Magn.*, vol. 47, no. 10, pp. 3280–3283, Oct. 2011.

[4] A. M. El-Refaie, T. M. Jahns, P. J. McCleer, and J. W. McKeever, "Experimental verification of optimal flux weakening in surface PM machines using concentrated windings," *IEEE Trans. Ind. Appl.*, vol. 42, no. 2, pp. 443–453, Mar./Apr. 2006.

[5] Y. Yoon, S. Sul, S. Morimoto, and K. Ide, "High-bandwidth sensorless algorithm for AC machines based on square-wave-type voltage injection," *IEEE Trans. Ind. Appl.*, vol. 47, no. 3, pp. 1361–1370, May/Jun. 2011.

[6] S. K. Kommuri, K. C. Veluvolu, M. Defoort, and Y. C. Soh, "Higher-order sliding mode observer for speed and position estimation in PMSM," *Math. Problems Eng.*, vol. 2014, pp. 1–12, 2014.

[7] H. Lee and J. Lee, "Design of iterative sliding mode observer for sensorless PMSM control," *IEEE Trans. Control Syst. Technol.*, vol. 21, no. 4, pp. 1394–1399, Jul. 2013.

[8] K. C. Veluvolu and C. S. Yeng, "High-gain observers with sliding mode for state and unknown input estimations," *IEEE Trans. Ind. Electron.*,vol. 56, no. 9, pp. 3386–3393, Sep. 2009.

[9] Y. Fan, L. Zhang, M. Cheng, and K. T. Chau, "Sensorless SVPWM-FADTC of a new flux-modulated permanent-magnet wheel motor based on a wide-speed sliding mode observer," *IEEE Trans. Ind. Electron.*, vol. 62, no. 5, pp. 3143–3151, May 2015.

[10] W. Xu, J. Zhu, Y. Zhang, Y. Guo, and G. Lei, "New axial laminated-structure flux-switching permanent magnet machine with 6/7 poles," *IEEE Trans. Magn.*, vol. 47, no. 10, pp. 2823–2826, Oct. 2011.

[11] W. Xu, G. Lei, T. Wang, X. Yu, J. Zhu, and Y. Guo, "Theoretical research on new laminated structure flux switching permanent magnet machine for novel topologic plug-in hybrid electrical vehicle," *IEEE Trans. Magn.*, vol. 48, no. 11, pp. 4050–4053, Nov. 2012.

[12] K. Atallah and D. Howe, "A novel high-performance magnetic gear," *IEEE Trans. Magn.*, vol. 37, no. 4, pp. 2844–2846, Jul. 2001.